

Supporting information for

ORIGINAL ARTICLE

Impact of particle size and pH on protein corona formation of solid lipid nanoparticles: a proof-of-concept study

Wenhao Wang^{a,†}, Zhengwei Huang^{a,†}, Yanbei Li^a, Wenhua Wang^a, Jiayu Shi^a,

Fangqin Fu^b, Ying Huang^{b,*}, Xin Pan^a, Chuanbin Wu^{a,*}

^a*School of Pharmaceutical Sciences, Sun Yat-Sen University, Guangzhou 510006, China*

^b*College of Pharmacy, Jinan University, Guangzhou 511443, China*

*Corresponding authors. Tel.: +86 20 39943427, fax: +86 020 39943115 (Ying Huang); Tel./fax: +86 20 39943120 (Chuanbin Wu).

E-mail addresses: huangy2007@jnu.edu.cn (Ying Huang), wuchuanb@mail.sysu.edu.cn (Chuanbin Wu).

† These authors made equal contributions to this paper.

1. Preparation and characterization of SLNS

1.1. Results

Table S1 Formulation composition and process parameters of SLNS.

Formulation	CP amount (g)	Tween 80 content (% <i>, w/v</i>)	Tween 80 volume (mL)	Homogenization pressure (bar)	Homogenization cycle	Homogenization temperature (°C)
SLNS1	1.5	2	50	1250	20	70
SLNS2	3.5	0.5	50	750	20	70
SLNS3	9.5	0.5	50	750	55	80

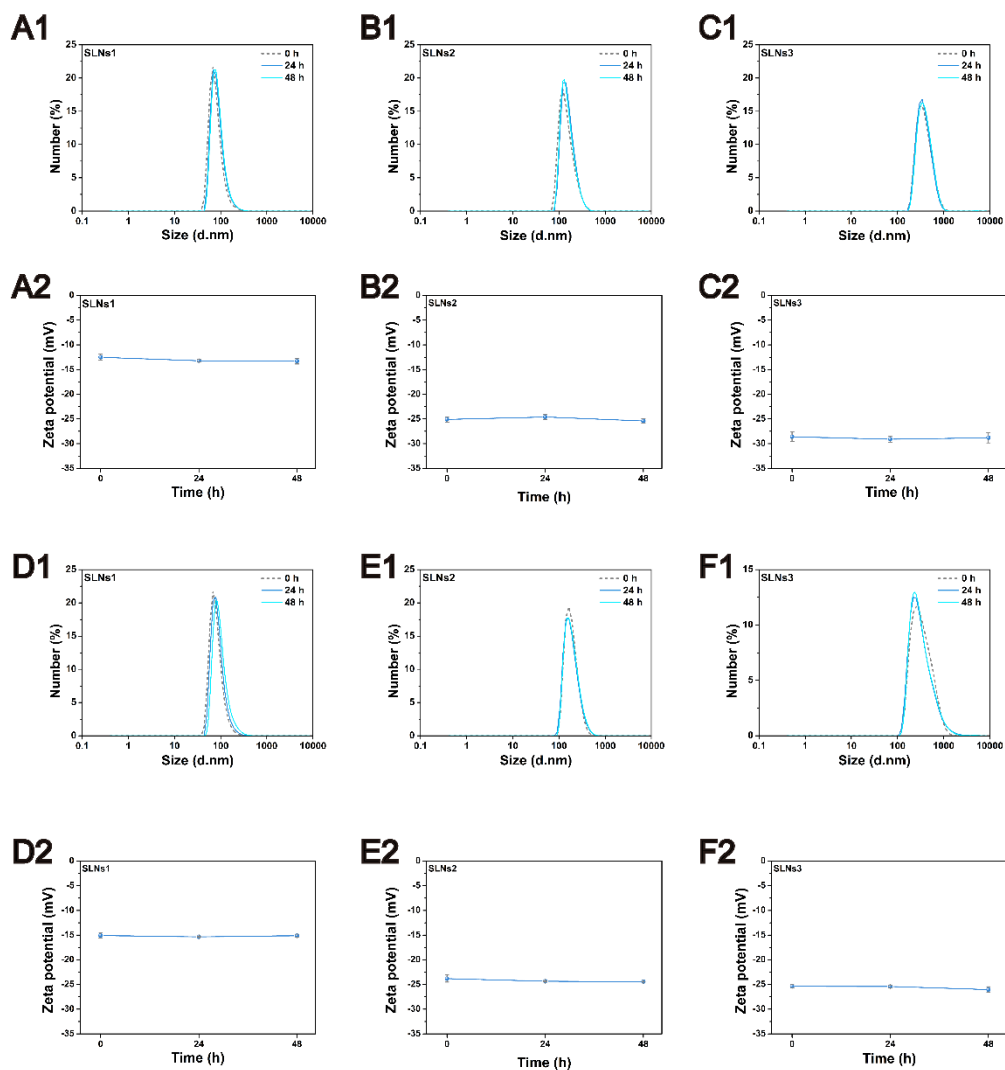


Figure S1 The storage stability of SLNS in different pH: the particle size distribution (1) and Zeta potential (2) of SLNS1(A), SLNS2 (B) and SLNS3 (C) in pH 6.0 and SLNS1 (D), SLNS2 (E) and SLNS3 (F) in pH 7.4. (Data are expressed as mean \pm SD, $n=3$).

2. DLS and Zeta-potential measurements in pH 6.0 and 7.4

2.1. Results

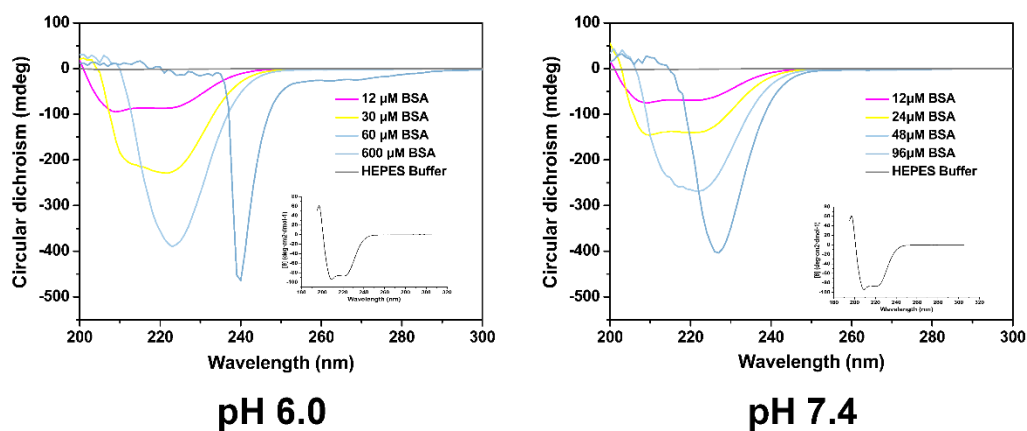


Figure S2 The CD spectra of different concentration BSA in HEPES buffer in pH 6.0 and 7.4.

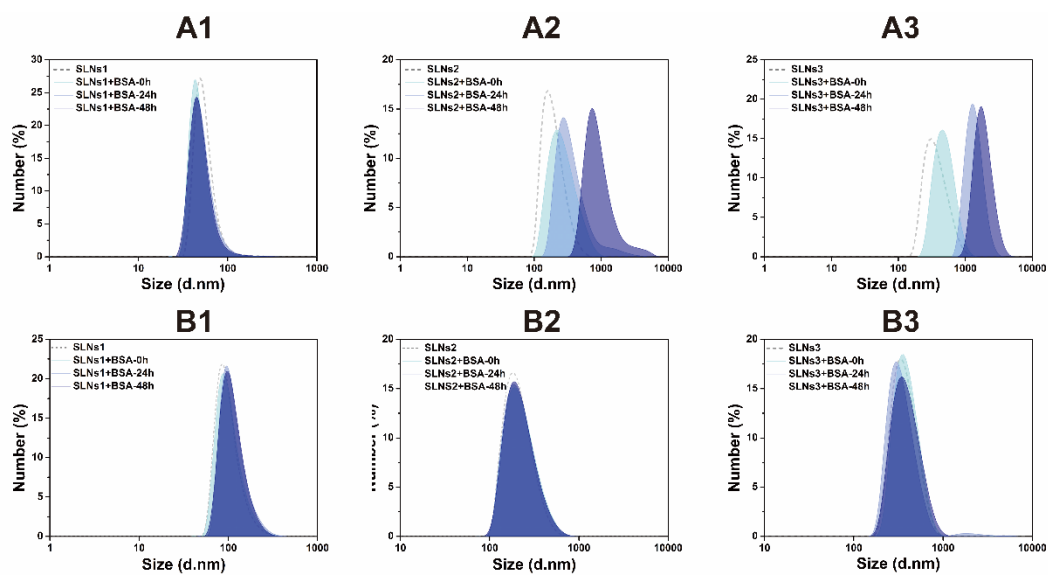


Figure S3 The size distribution of BSA incubated SLNS in pH 6.0 (A) and pH 7.4 (B) over time.

3. The BSA corona formation in pH 7.4

3.1. Methods

3.1.1. Raman spectroscopy and TLC analyze

To further confirm the formation of protein corona in pH 7.4, the Raman spectroscopy and thin layer chromatography (TLC) method were employed. Specifically, the Raman spectra from 50 to 4000 cm^{-1} of SLNS in the presence or absence of BSA were recorded by a Laser Micro-Raman Spectrometer (Renishaw inVia, Renishaw, UK) with the excitation wavelength set at 514.5 nm.

As for the TLC method, the ACQ probe P2 loaded SLNS2 were selected as the example to incubated with BSA for 4 h. Then, the P2 loaded SLNS2 with or without BSA were introduced to a silica gel G pre-coated plate and the water/acetonitrile mixture (1:2, *v/v*) was selected as eluent. The fluorescence distribution of the plate was recorded and analyzed by an *in vivo* imaging system (NightOWL II LB983, BERTHOLD, Germany).

3.2. Results

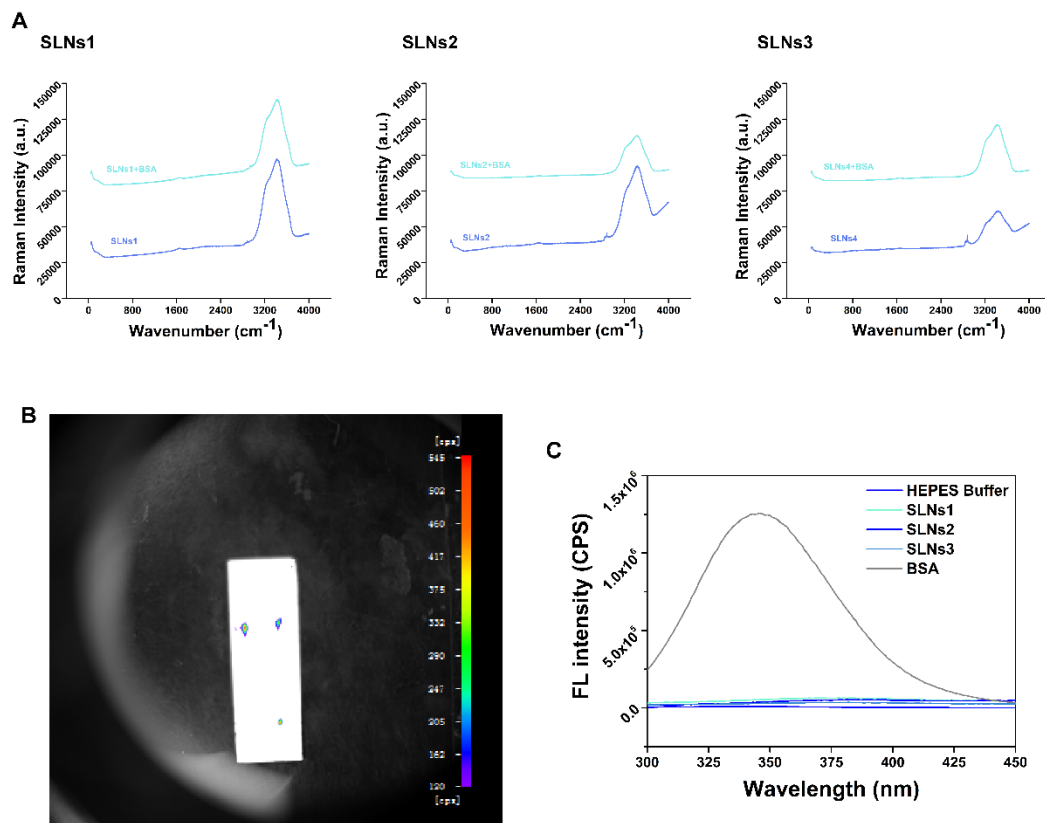


Figure S4 The Raman spectra of SLNS-BSA in pH 7.4 (A) and the fluorescence distribution of the TLC plate (B). The fluorescence spectra of HEPES buffer, SLNS and BSA (C).

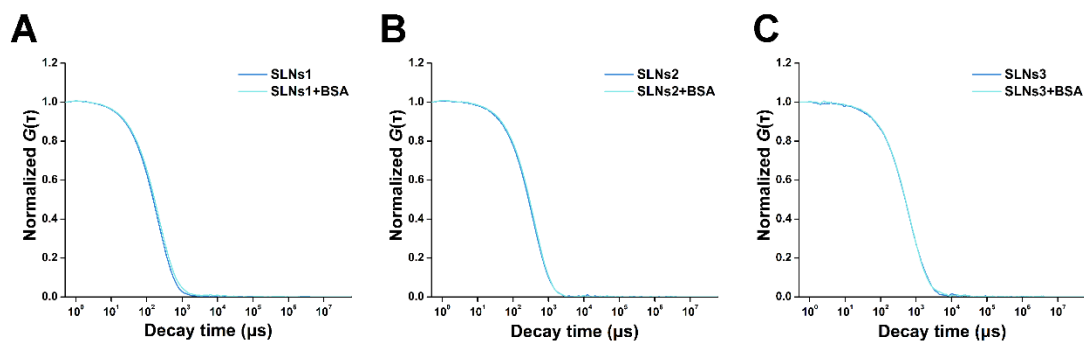


Figure S5 The normalized ACFs curves of SLNS-BSA in pH 7.4.

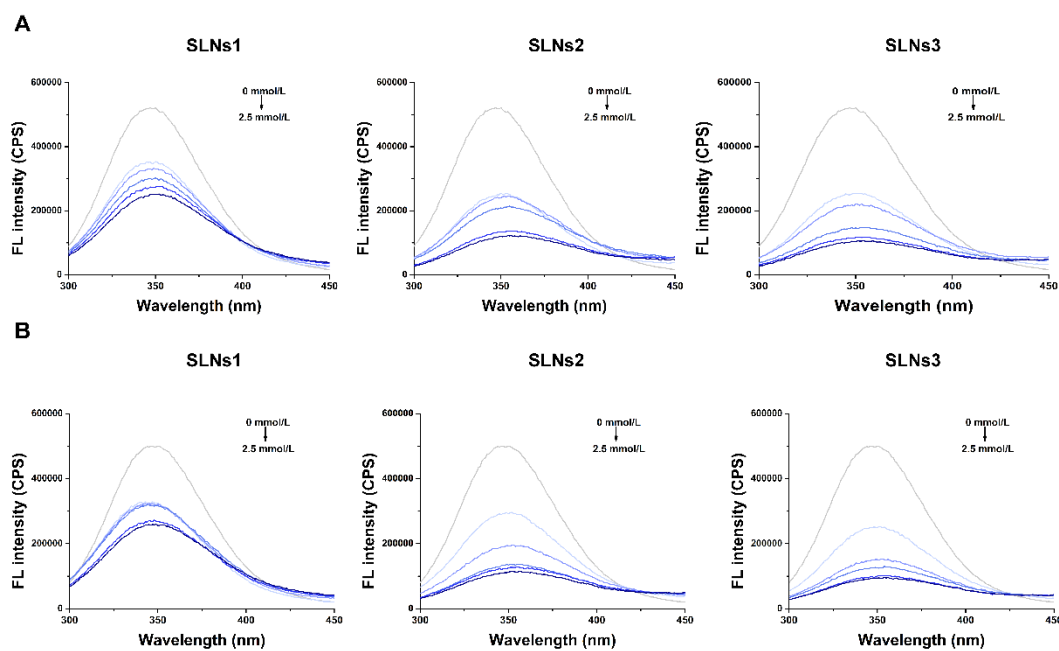


Figure S6 The fluorescence quenching spectra of BSA after incubation with different concentration SLNS in 0 (A) and 24 h (B).

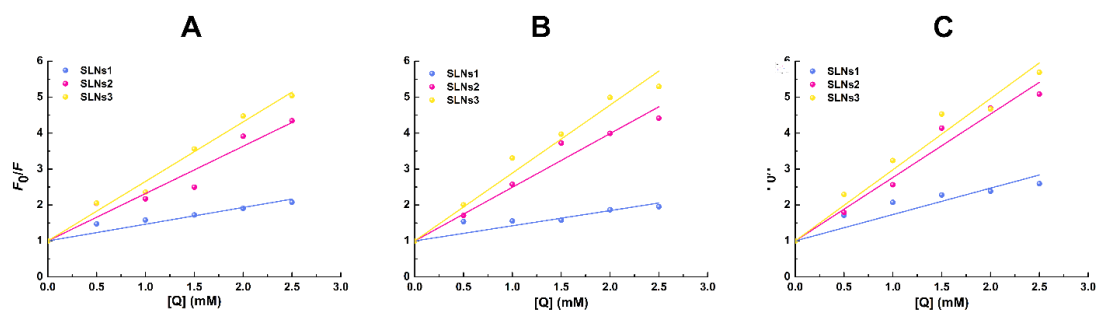


Figure S7 The fluorescence quenching plots of BSA in the presence of SLNS in 0 (A), 24 (B) and 48 h (C).

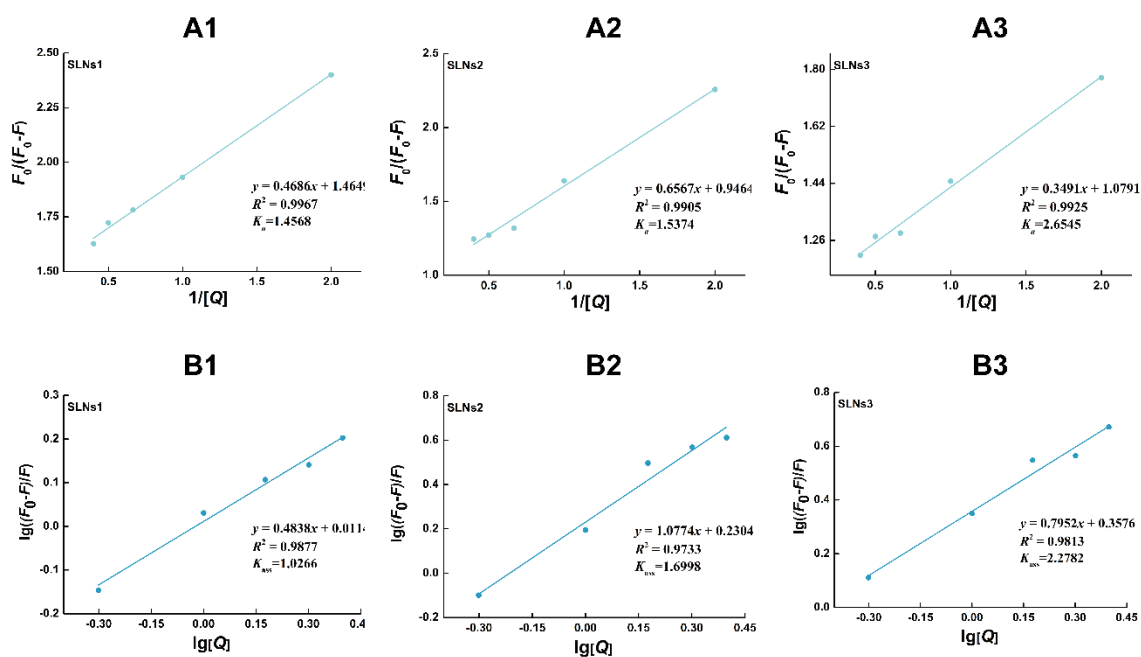


Figure S8 The Scatchard plots (A) and the modified Stern–Volmer plots (B) of SLNS-BSA.

4. Conformational change of BSA

4.1. Results

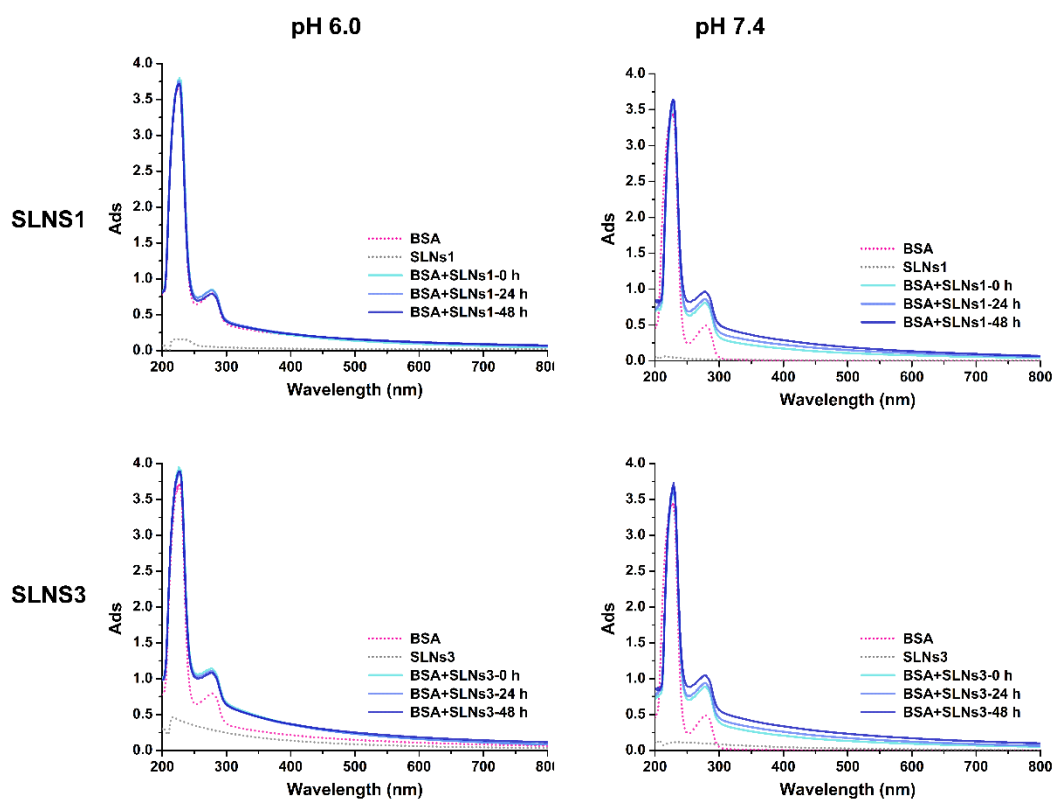


Figure S9 The UV–Vis spectra of BSA in the absence and presence of SLNS in pH 6.0 and 7.4.

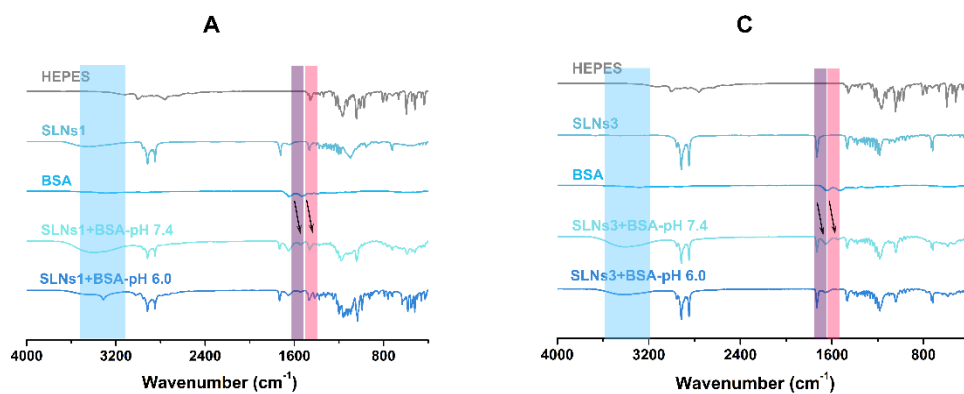


Figure S10 The FTIR spectra of BSA in the absence and presence of SLNS in different pH.

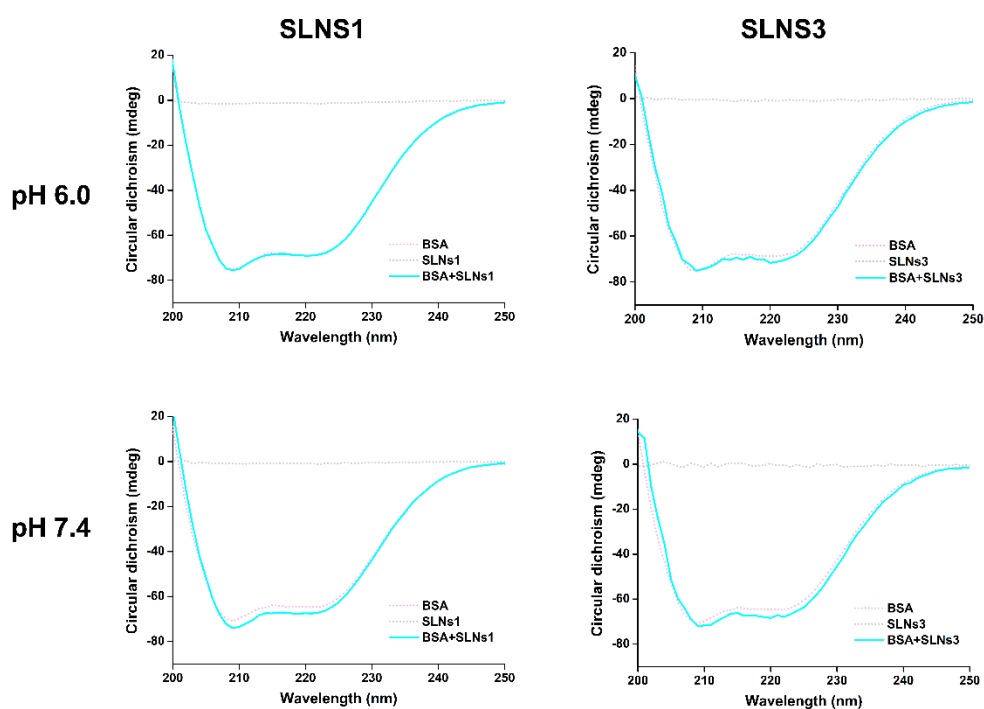


Figure S11 The CD spectra of BSA in the absence and presence of SLNS in pH 6.0 and 7.4.

5. The structural change of SLNS

5.1. Methods

The POM was set up using Linkam hot stage (THM S600, Waterfield, UK) combined with a Nikon polarizing microscopy (Nikon eclipse lv100N pol, Tokyo, Japan). CP and Tween 80 were heated to 80 °C and then cool to room temperature on the hot stage to simulate the preparation process of SLNS and imaged. Then, the POM image

of SLNS was taken to observe their crystalline structure. Then, the ACQ probe P2-loaded SLNS and P4-loaded SLNS were employed to detect the integrity of SLNS after interaction with BSA. The fluorescence intensity of P2-SLNS at 715 nm and P4-SLNS at 660 nm before and after incubation with BSA for 48 h was determined with excitation performed at 710 and 620 nm, respectively.

5.2. Results and discussion

5.2.1. Integrity of nanoparticles

Most previous researches only paid their attention to the structural change of protein upon interaction with NPs¹, but those on the topic whether the nanoparticles remain integrity upon interaction lagged far behind. As the SLNS was a kind of soft materials, the morphologic changes of SLNS such as fusion or rupture might be induced by the protein corona formation. The ACQ probes P2 and P4 were employed to detect the integrity of SLNS in this study. Due to the occurrence of π - π stacking, ACQ probes are quenched by the formation of excimers and exciplexes in aqueous environment. Thus, when dispersed in lipid matrix, the probes were supposed to be illuminated (on), while they would turn to be quenched (off) when released to water. The “on-off” switchable ability makes it a great choice for monitoring the integrity of lipid-based NPs²⁻⁵.

The fluorescence intensities of P2- or P4-loaded SLNS before and after incubation with BSA in pH 6.0 and 7.4 were determined. As shown in Fig. S12A, no significant difference was found in the fluorescence intensities between pristine SLNS and BSA incubated SLNS, demonstrating the negligible leak of ACQ probe from SLNS. Thus, it was suggested that the integrity of SLNS was not damaged by the protein corona formation and there was also no lipid core fusion in both pH.

5.2.2. POM images of SLNS

In theory, the SLNS might bear a core-shell structure. This was because Tween 80 with stronger polarity would distribute in the shell with high affinity towards the aqueous solution, while CP with weaker polarity would distribute in the core. The POM images of CP, Tween 80 and SLNS were taken to further prove the core-shell structure of SLNS. As the temperature is the main factor affecting the crystalline state,

a melting-cooling procedure was carried out to simulate the preparation process of SLNS. As shown in Fig. S12B, the obvious colorful bright zone due to the optical anisotropy of the crystals was found in POM images of CP after the melting-cooling procedure. It was indicated that the CP existed in crystalline form. However, no colorful bright zone was found in the POM images of Tween 80, suggesting the amorphous form of Tween 80. Hence, the non-crystal images of SLNS revealed that the crystalline CP was embedded in the amorphous Tween 80, proving the core-shell structure of SLNS.

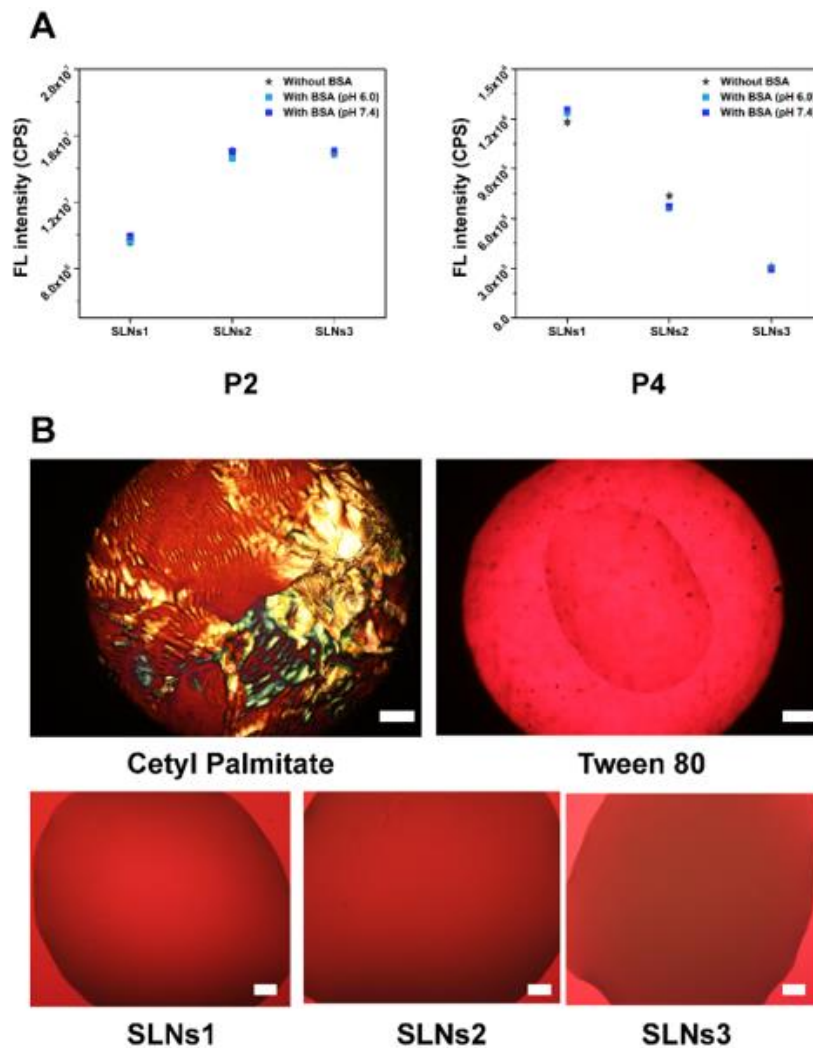


Figure S12 The fluorescence intensities of P2- or P4-loaded SLNS before and after incubation with BSA in different pH (A). The POM images of Tween 80, CP and SLNS (B). Scale bar=200 μm , Data are expressed as mean \pm SD, $n=3$.

6. Mechanism studies

6.1. Methods

6.1.1. Interaction between Tween 80 and BSA

The molecular docking of Tween 80 and BSA was carried out using AutoDock molecular docking technique. Specifically, the chemical structures of Tween 80 and BSA were converted to pdbqt files using Mgtools1.5.6. Then, the pdbqt files of BSA and Tween 80 were processed by Autogrid software. A box of 126×98×110 with center $x = 8.427$, center $y = 21.626$, center $z = 105.299$ was built, which was saved into a .gpf file. Then, the .glg file was generated from the .gpf file through autogrid4.exe operation. Finally, the Autodock4 software was utilized to simulate the molecular interaction with 100 times operations using the Lamarckian genetic algorithm.

The interaction of Tween 80 and BSA was analyzed through ITC. The ITC methods were described above. In brief, the 12 $\mu\text{mol/L}$ BSA solution was titrated to 1.2 $\mu\text{mol/L}$ Tween 80 solution and the data of heat vs. molar ratio were recorded.

6.1.2. Interaction of SLNS with other proteins with different PI

Then, four proteins with different isoelectric points (PI) including ovalbumin (OVA), BSA, trypsinogen (Try) and lysozyme (Lys) were chosen to incubate with SLNS. The D_H of SLNS with or without incubating with proteins for 4 h was determined by a high flux plates reading dynamic laser scattering method using a DynaPro Plate Reader II (WYATT, Santa Barbara, CA, USA). The samples were introduced carefully into the 96-well plate and the D_H of each well was determined. The ratio of D_H of pristine SLNS and protein-SLNS complexes were calculated and analyzed.

6.2. Results and discussion

Table S2 The thermodynamic parameters of BSA-SLNS in pH 7.4.

Parameter	SLNS1	SLNS2	SLNS3
<i>N</i>	0.75	0.516	0.24
<i>K</i>	1.27×10^6	7.10×10^5	3.19×10^6
ΔH (kJ/mol)	-1.639×10^5	-2.478×10^5	-8.006×10^4
ΔS (kJ/mol/K)	-501	-772	-228

6.2.1. Interaction between Tween 80 and BSA

The interaction between BSA and Tween 80 was further exploited by the AutoDock molecular docking technique. The amino acid interaction sites of BSA–Tween 80 were illustrated in Fig. S13A, which showed that Pro179, Lys180, Lys187, Glu291, Lys294, Tyr340, Ala341, Pro446 and Cys447 were the main amino acid residues of BSA interacting with Tween 80. In addition, the adsorption of BSA on Tween 80 was mainly driven by hydrophobic effect, van der Waals force and hydrogen bonding. In summary, the formation of BSA–SLNS complex may be partly attributed to the BSA–Tween 80 interaction including hydrophobic effect, van der Waals force and hydrogen bonding. To further confirm the interaction between BSA and Tween 80, the ITC experiment was carried out. The ITC results (Supporting information Fig. S13B) show that the interaction between BSA and Tween 80 was multifactorial, and the hydrophobic effect, van der Waals force and hydrogen bonding were involved in the process. Thus, the interaction between BSA and Tween 80 was proved to be an important part during the protein corona formation process.

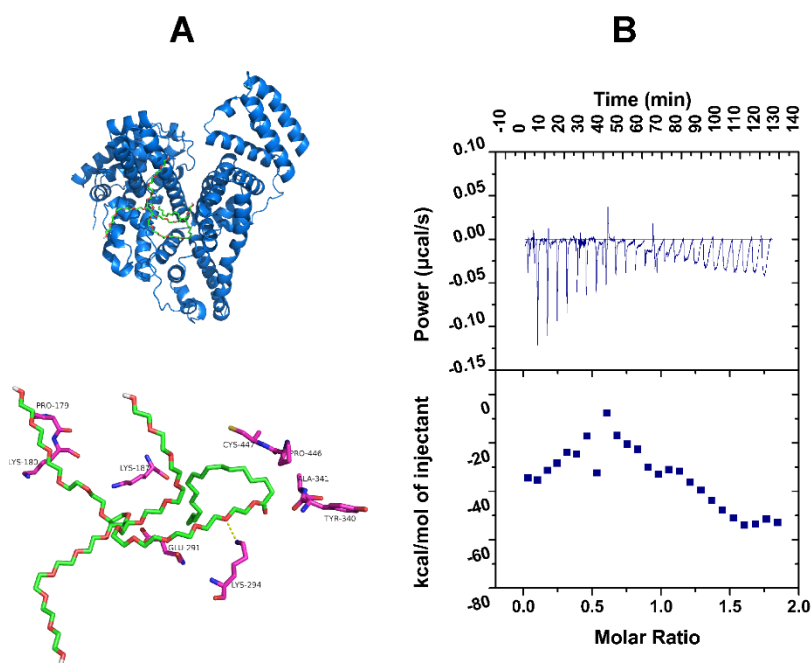


Figure S13 The AutoDock molecular docking results of Tween 80-BSA (A). The ITC power-time data (upper panel) and the subsequent binding isotherm of BSA to Tween 80 (lower panel).

6.2.2. Interaction of SLNS with other proteins with different PI

The Zeta-potential of BSA-SLNS complexes in pH 6.0 was significantly lower than that in pH 7.4, demonstrating that the stronger electrostatic attraction between protein corona coated SLNS in pH 6.0 might be attributed to the process of aggregation and colloidal instability. Because the net charge of protein was positive when pH was below the PI and *vice versa*, which affected the surface charge of protein corona coated SLNS and thus the electrostatic attraction between them. Four kinds of proteins with different PI including OVA (PI 4.7), BSA (PI 4.7), Try (PI 9.3) and Lys (PI 11.1) were employed to detect the relationship between protein PI and the aggregation state of SLNS upon addition of proteins. As shown in Fig. S14, the addition of Try and Lys with high PI led to the aggregation of SLNS in both pH, while the addition of OVA and BSA with low PI only caused aggregation in pH 6.0 but not in pH 7.4. In addition, an interesting phenomenon showed that SLNS1 which exhibited great colloidal stability incubating with BSA was also aggregated after incubation with Try and Lys in pH 6.0. The reason might be a large amount of Try and

Lys with high positive net charge in pH 6.0 adsorbed on the negatively charged SLNS1 and masked the protection effect of hydrophilic surface against the protein corona caused aggregation. These results imply that the electrostatic attraction is a vital part of the interaction among NPs, proteins and protein corona coated NPs in pH 6.0, which is in line with the previous reports^{6,7}.

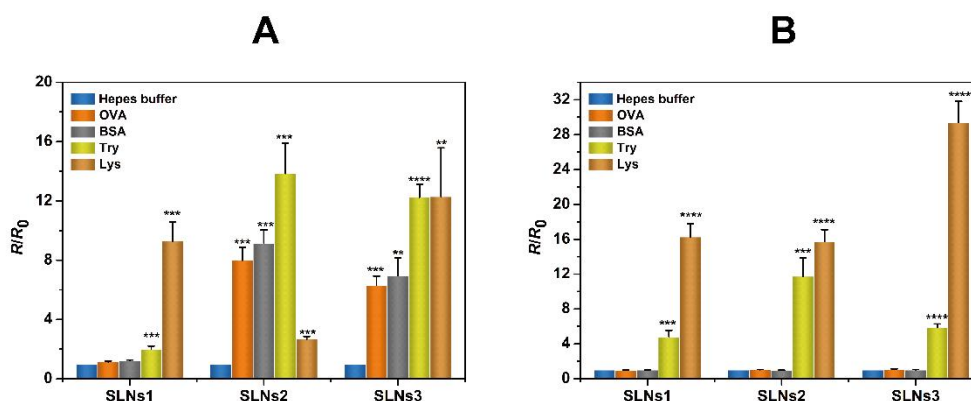


Figure S14 The R/R_0 of SLNS after incubation with proteins in pH 6.0 (A) or pH 7.4 (B). * $P < 0.05$; ** $P < 0.01$; *** $P < 0.001$; **** $P < 0.0001$, Data are expressed as mean \pm SD, $n=3$, HEPES buffer vs. other groups.

References

1. del Caño R, Mateus L, Sánchez-Obrero G, Sevilla JM, Madueño R, Blázquez M, et al. Hemoglobin bioconjugates with surface-protected gold nanoparticles in aqueous media: the stability depends on solution pH and protein properties. *J Colloid Interface Sci* 2017;**505**:1165–71.
2. Feng YH, He HS, Li FQ, Lu Y, Qi JP, Wu W. An update on the role of nanovehicles in nose-to-brain drug delivery. *Drug Discov Today* 2018;**23**:1079–88.
3. Ahmad E, Feng YH, Qi JP, Fan WF, Ma YH, He HS, et al. Evidence of nose-to-brain delivery of nanoemulsions: cargoes but not vehicles. *Nanoscale* 2017;**9**(3):1174–83.
4. Hu XW, Zhang J, Yu Z, Xie YC, He HS, Qi JP, et al. Environment-responsive aza-BODIPY dyes quenching in water as potential probes to visualize the *in vivo* fate of lipid-based nanocarriers. *Nanomedicine Nanotechnology, Biol Med* 2015;**11**:1939–48.

5. He HS, Xie YC, Lv YJ, Qi JP, Dong XC, Zhao WL, et al. Bioimaging of Intact polycaprolactone nanoparticles using aggregation-caused quenching probes: size-dependent translocation *via* oral delivery. *Adv Healthc Mater* 2018;**1800711**:1–11.
6. Oh N, Park JH. Endocytosis and exocytosis of nanoparticles in mammalian cells. *Int J Nanomedicine* 2014;**9** suppl 1:51–63.
7. Beck-Broichsitter M, Ruppert C, Schmehl T, Guenther A, Betz T, Bakowsky U, et al. Biophysical investigation of pulmonary surfactant surface properties upon contact with polymeric nanoparticles *in vitro*. *Nanomed Nanotechnol Biol Med* 2011;**7**:341–50.